Analysis of the temperature performance of type-II interband cascade lasers

Mikhail V. Kisin,[a] Sergey D. Suchalkin, and Gregory Belenky
Department of Electrical and Computer Engineering, State University of New York at Stony Brook, Stony Brook, New York 11794

John D. Bruno
Maxion Technologies Incorporated, Hyattsville, Maryland 20782

Richard Tober
Army Research Laboratory, Adelphi, Maryland 20873

Serge Luryi
Department of Electrical and Computer Engineering, State University of New York at Stony Brook, Stony Brook, New York 11794

(Received 8 December 2003; accepted 7 September 2004)

The temperature performance of type-II semiconductor lasers has been analyzed by comparing the temperature-concentration dependence for a charge-carrier subsystem at the threshold with steady-state temperature-concentration relationship implied by the carrier heating process. The low material gain characteristic of type-II heterostructures and the high resistance of the thermal link to the heat sink are primarily responsible for limiting the continuous-wave laser operation to low temperatures. We show also that the number of cascades for type-II interband cascade lasers can be optimized with respect to the highest achievable operating temperature. © *2004 American Institute of Physics*. [DOI: 10.1063/1.1814432]

In midinfrared (MIR) quantum-well lasers, the optical gain $g(n_e, T_e)$ is a strong function of both the carrier concentration and the carrier temperature. Any increase of the laser operating temperature is accompanied by a compensating rise of the carrier concentration in the active region, which in electrically injected lasers implies a corresponding increase of the threshold current. The latter in turn induces additional Joule heating, while the concentration buildup enhances the nonradiative (Auger) current. At some point, this leads to a lasing failure. For design purposes, it is very important to understand the main "trigger" mechanism of such a failure—whether it is the Joule heating of the crystal lattice or the Auger-related heating of the electron subsystem. In this work, we describe a method that allows for a comparison of the physical effects most critical for high-temperature operation of semiconductor lasers and apply it to type-II interband cascade lasers (ICLs).[1] Our approach is based on matching the temperature-concentration relation obtained from the laser threshold condition with an independent relation describing the laser heating characteristics in the continuous-wave (cw) operating regime.[2,3] At high injection levels, typical for near-room-temperature operation, the Auger recombination is essentially responsible for the threshold current in MIR lasers and is, therefore, the basic physical mechanism limiting their cw operation to low temperatures.[4] We show, however, that the high value of the specific thermal resistance in antimonide-based ICLs (Ref. 1) can equally determine the ultimate cause of the device failure. This agrees with our experimental data for 3.7 μm type-II cascade lasers.

At the lasing threshold, the modal optical gain g_{mod} must compensate for the total optical loss α_{tot}. In semiconductor lasers, both quantities can generally be functions of the electron concentration and temperature, n_e and T_e. Therefore, the lasing threshold condition, $g_{\mathrm{mod}}(n_e, T_e) = \alpha_{\mathrm{tot}}(n_e, T_e)$, implies a certain relationship between the threshold carrier concentration n_{th} and temperature T_{th}, which is a curve $T_{\mathrm{th}}(n_{\mathrm{th}})$ in the $n_e - T_e$ coordinate plane. In the simplest model considered in this work, we shall assume that the optical loss is not a strong function of n_e and T_e, which is a reasonable approximation for type-II ICLs.[5,6] In this case, the dependence $T_{\mathrm{th}}(n_{\mathrm{th}})$ represents the "isogain" curve g_{mod}=constant. Another relationship in the $n_e - T_e$ plane results from the consideration of carrier heating. Carrier concentration in the active region is determined by the injection current, which in turn strongly affects the electron temperature. The energy balance equation thus defines a curve $T_e(n_e)$, which represents all possible steady states of the system. This curve must somewhere match the threshold isogain line $T_{\mathrm{th}}(n_{\mathrm{th}})$, so that the intersection between these two curves, $T_{\mathrm{th}}(n_{\mathrm{th}})$ and $T_e(n_e)$, determines the laser operating point. If there is no intersection, the device will not lase at any injection current.

The sheet carrier concentration n in the active quantum wells determines the injected current density $J = J_R + J_{\mathrm{SRH}} + J_A$, which is a combination of both the radiative and nonradiative components. The current component $J_{\mathrm{SRH}} = qAn$ accounts for the Shockley–Read–Hall (SRH) recombination at interfaces and impurities. Reported values[7,8] of the coefficient A are of the order of $10^8 \mathrm{s}^{-1}$. They are characterized by negligible temperature dependence and do not vary with the quantum-well width. The last component of J is the Auger recombination current, $J_A = Cn_{\mathrm{eff}}^3$. We assume that the Auger process is controlled by the 2D carrier concentration n in the active quantum wells, so that the effective 3D concentration used in the calculation can be estimated with respect to the combined widths of the adjacent electron and hole quantum wells as $n_{\mathrm{eff}} = n/(d_e + d_h)$. The reported Auger recombination

[a]Electronic mail: mvk@ece.sunysb.edu

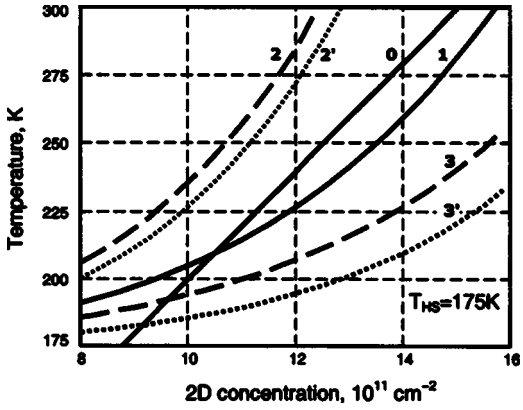

FIG. 1. Graphical analysis of the temperature performance of type-II ICL in the n_e-T_e plane. Solid curve **0** shows the isogain line $T_{th}(n_{th})$. Curves **1**–**3** show equilibrium electron temperature-concentration dependence $T_e(n_e)$; (**1**) $C=5\times10^{-27}$ cm^6/s, $\rho_T=15$ K cm^2/kW; (**2**–**3**) $C=10^{-26}$ cm^6/s; thermoresistance values: $\rho_T=15$ K cm^2/kW (curve **2**) and $\rho_T=3$ K cm^2/kW (curve **3**). The dotted lines **2**′ and **3**′ show the equilibrium lattice temperature $T_L(n_e)$ for high and low thermoresistance values.

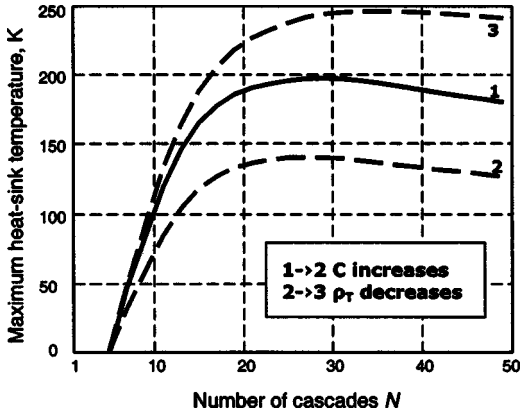

FIG. 2. Maximum heat-sink temperature vs number of cascades N for type-II ICLs. The curve assignment is the same as in Fig. 1. Dashed curve **2** demonstrates the strong depression of the maximum operation temperature by Auger recombination (compare with curve **1**). Curve **3** illustrates the recovering effect of the lower thermal resistance. Room-temperature operation becomes feasible at the lowest thermoresistance value $\rho_T<3$ K cm^2/kW even for an Auger coefficient as high as $C=10^{-26}$ cm^6/s.

rate in type-II InAs/GaInSb multiple quantum wells and superlattices is nearly an order of magnitude lower than the typical values for type-I laser heterostructures in the same spectral region 3–5 μm.[8] In type-II heterostructures at $\lambda\sim4$ μm, the reported values[7–9] of 3D Auger coefficient C are in the range 10^{-27}–10^{-26} cm^6 s^{-1}. While there is still a controversy about the temperature dependence of the Auger process in type-II heterostructures designed for MIR lasers,[10,11] we shall assume thresholdless Auger recombination[11] and use representative room-temperature values[8] of C.

The Auger recombination is also responsible for carrier heating. We assume that each act of nonradiative recombination transfers back into the carrier subsystem an energy of the order of the optical quantum $h\nu$. The energy balance then gives a simple estimate of the difference between the carrier and the lattice temperatures, $T_e-T_L=h\nu(J_A\tau_\varepsilon/qn)$. The energy relaxation time τ_ε is assumed here to be common for both electrons and holes, and uniform throughout the active region. The lattice temperature T_L in cw regime is primarily determined by Joule heating, $T_L=T_{HS}+\rho_T JV$, where T_{HS} is the heat-sink temperature and ρ_T is the specific thermal resistance of the laser heterostructure. The voltage drop at the threshold, $V=\rho_s J+Nh\nu/q$, is determined primarily by the cascaded active regions and also by the specific series resistance ρ_s associated with the injection regions and the waveguide cladding regions. In cascaded structures, the series resistance ρ_s has two components, $\rho_s=N\rho_{inj}+\rho_{s0}$, where the first term is the N dependent active region resistance associated mostly with the injectors, and the second term represents the contribution of the waveguide cladding layers and therefore does not depend on N. At the moment, we lack detailed information about series resistance in structures with different numbers of stages, and we assign the total value of the series resistance to the N independent part.

Figure 1 illustrates our method of analysis. The bold straight line **0** (isogain line) represents the threshold condition $T_{th}(n_{th})$ for a typical value of the internal optical loss $\alpha_{int}=20$ cm^{-1} at the lasing wavelength $\lambda=4$ μm.[5,6] Curves **1**–**3** show the equilibrium electron temperature $T_e(n_e)$ calculated for $\tau_\varepsilon=1$ ps. The typical value of the specific series resistance taken here is $\rho_s=3$ mΩ cm^2 (Ref. 1), and the heat-sink temperature is $T_{HS}=175$ K. Curves **1** and **2** have been obtained using the same high value of the specific thermal resistance, $\rho_T=15$ K cm^2/kW, which is typical for wide-stripe ICL.[1] Auger coefficients in these two calculations differ by a factor of 2, $C=5\times10^{-27}$ cm^6/s (curve **1**) and $C=10^{-26}$ cm^6/s (curve **2**). The SRH recombination coefficient was taken at a typical value of $A=10^8$ s^{-1} (Ref. 8). The intersection of an electron temperature curve with the threshold isogain line defines the laser threshold operating point. For the lower value of the Auger recombination rate, there is a robust lasing generation represented by the intersection of the curve **1** and isogain line **0**. Due to the low value of the optical gain in a type-II ICL, only a two-fold increase of the Auger coefficient brings the device out of operation, so that curve **2** shows no intersection with isogain line **0**. Curve **3** demonstrates the recovering effect of the lower thermal resistance ρ_T. Remarkably, as small as a three-fold decrease of the thermal resistance ρ_T brings the laser back into the operating range even for the Auger coefficient as high as $C=10^{-26}$ cm^6/s. Calculation shows that laser generation is securely recovered (isogain line reappears) already at $\rho_T=5$ K cm^2/kW. Dotted curves **2**′ and **3**′ illustrate the equilibrium lattice overheating $T_L(n_e)$ in the active region at high and low thermoresistance values. It is readily seen that the electron heating plays only a secondary role in the overall device overheating, while the lattice temperature increase apparently dominates the process at high thermoresistance values (compare the dashed and dotted curves **2**–**2**′ and **3**–**3**′).

When the threshold isogain line $T_{th}(n_{th})$ is tangent to the electron temperature curve $T_e(n_e)$, the laser operation becomes marginal, so that this regime corresponds to the highest operating (heat-sink) temperature T_{max} achievable for a given device. Figure 2 shows the calculated dependence of the maximum operating temperature T_{max} on the number of cascade stages N. We assume that both the optical loss and the series resistance in the ICL heterostructure originate in the cladding and contact layers, thus keeping those quantities N independent in our illustrative calculations. In this situation, the most important consequence of the increase of the number of stages is the corresponding increase in the confinement factor and the modal gain which accounts for the sharp increase of the temperature performance with N at

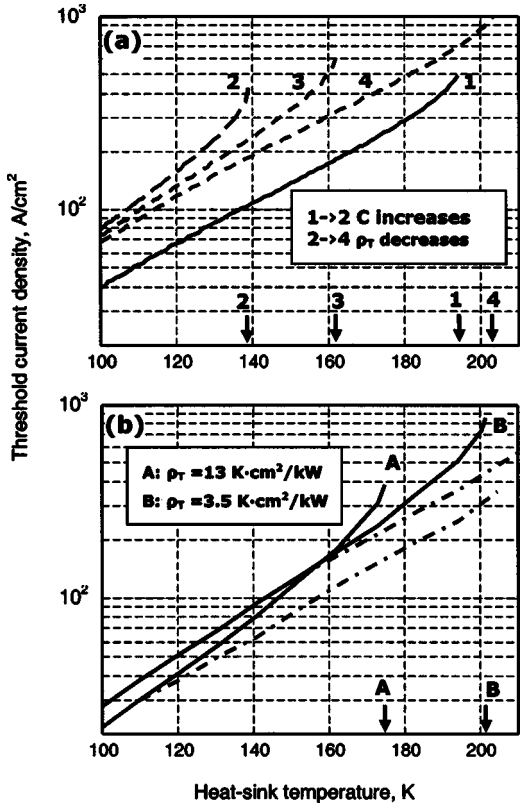

FIG. 3. Threshold current density J_{th} as a function of heat-sink temperature T_{HS}. (**a**) Calculated dependencies; for curves **1** and **2**, the curve assignment is the same as in Fig. 1. Curves 3 and 4 correspond to $\rho_T=10$ and 5 K cm^2/kW. The maximum achievable operating (heat-sink) temperature for each parameter set (**1**–**4**) is indicated by arrows: (**1**) $T_{max}=194$ K, (**2**) $T_{max}=139$ K, (**3**) $T_{max}=162$ K, and (**4**) $T_{max}=204$ K. (**b**) Experimental dependencies measured in cw mode for two devices with different mesa widths: 35 μm (curve **A**) and 8 μm (curve **B**). Dashed–dotted lines show data from pulsed operation.

small $N<20$. A further increase in the number of stages, however, proportionally increases the threshold voltage and the heat dissipation in the active region. Since both the confinement factor and the modal gain saturate at large N, this leads to device overheating and gradually decreases the maximum operating temperature T_{max} for $N>30$. Note that in unipolar quantum cascade lasers (QCLs), where the transparency current is negligible, the increase of the number of cascades is accompanied by a proportional decrease of the threshold current which results in a pronounced minimum in the dissipated electrical power at $N\approx 20$.[12] In ICLs, due to the higher value of the transparency current, the threshold current does not decrease so dramatically with N, so that the power dissipation at the threshold does not reveal such a minimum. Nevertheless, an optimum number of stages exists in an ICL, although it is not as sharply peaked as it is in a QCL. The optimal number of ICL stages, which we define here with respect to the highest possible heat-sink temperature T_{max}, is in a rather wide range between 20 to 30 cascades, so that additional optimization with respect to the output optical power is possible.

Figure 3 shows the threshold current density versus the heat-sink temperature $J_{th}(T_{HS})$. The calculated dependencies shown in Fig. 3(a) again demonstrate the competitive effect of the Auger recombination and the heterostructure thermoresistance on the laser temperature performance. To illustrate experimentally the influence of the thermoresistance decrease on the laser temperature performance, we measured the threshold current in two ICL devices processed with different mesa widths, 35 μm and 8 μm [Fig. 3(b), curves **A** and **B**]. Both lasers are of similar design and emit at 3.7 μm. The different mesa width leads to a different thermal resistance and, therefore, affects the laser temperature performance. The thermal resistance and maximum operating temperature are $\rho_T=13$ K cm^2/kW and $T_{max}=175$ K for the 35 μm mesa device (**A**), and, correspondingly, $\rho_T=3.5$ K cm^2/kW and $T_{max}=205$ K for the 8 μm mesa device (**B**). The observed improvement of T_{max} agrees qualitatively with the predictions of our theoretical model thus illustrating its applicability. A more detailed quantitative comparison is complicated by the fact that the decrease of the mesa width additionally affects the threshold current by increasing the part of the surface recombination which is not included in our simple theoretical model.

In conclusion, we describe a simple method for analyzing the temperature performance of semiconductor lasers which is based on comparing the temperature-concentration dependence at the laser threshold with a steady-state temperature-concentration relationship obtained from carrier heating analysis. We use this method to highlight the physical effects most critical for the high-temperature operation of type-II ICLs in the 3–4 μm spectral region. We show that the low material gain and high value of the specific thermal resistance typical for antimonide-based cascade lasers are primarily responsible for limiting cw operation of these devices to low temperatures. We show also that the number of ICL cascades has an optimum with respect to the highest cw operating temperature, though the range of optimum values is rather wide, comprising 20 to 30 cascades.

This work was supported by the ARO Grant No. DAAD190310259 and MURI-AFOSR Grant No. F496200010331. Work at Maxion was supported by the ARL and by AFRL Contract No. F19628-02-C-0032.

[1] R. Q. Yang, J. L. Bradshaw, J. D. Bruno, J. T. Pham, and D. E. Wortman, IEEE J. Quantum Electron. **38**, 559 (2002).
[2] V. B. Gorfinkel, S. Luryi, and B. Gelmont, IEEE J. Quantum Electron. **32**, 1995 (1996).
[3] V. B. Gorfinkel, M. V. Kisin, and S. Luryi, Opt. Express **2**, 125 (1998).
[4] B. N. Murdin, Philos. Trans. R. Soc. London, Ser. A **359**, 459 (2001).
[5] S. Suchalkin, D. Westerfeld, D. Donetski, S. Luryi, G. Belenky, R. Martinelli, I. Vurgaftman, and J. R. Meyer, Appl. Phys. Lett. **80**, 2833 (2002).
[6] S. Suchalkin, J. Bruno, R. Tober, D. Westerfeld, M. Kisin, and G. Belenky, Appl. Phys. Lett. **83**, 1500 (2003).
[7] S. W. McCahon, S. A. Anson, D. J. Jang, M. E. Flatte, T. F. Boggess, D. H. Chow, T. C. Hasenberg, and C. H. Grein, Appl. Phys. Lett. **68**, 2135 (1996).
[8] J. R. Meyer, C. L. Felix, W. W. Bewley, I. Vurgaftman, E. H. Aifer, L. J. Olafsen, J. R. Lindle, C. A. Hoffman, M. J. Yang, B. R. Bennett, B. V. Shanabrook, H. Lee, C. H. Lin, S. S. Pei, and R. H. Miles, Appl. Phys. Lett. **73**, 2857 (1998).
[9] M. E. Flatte, C. H. Grein, T. C. Hasenberg, S. A. Anson, D. J. Jang, J. T. Olesberg, and T. F. Boggess, Phys. Rev. B **59**, 5745 (1999).
[10] D. J. Jang, M. E. Flatte, C. H. Grein, J. T. Olesberg, T. C. Hasenberg, and T. F. Boggess, Phys. Rev. B **58**, 13047 (1998).
[11] G. G. Zegrya and A. D. Andreev, JETP **82**, 328 (1996).
[12] C. Gmachl, F. Capasso, A. Tredicucci, D. L. Sivco, R. Kohler, A. L. Hutchinson, and A. Y. Cho, IEEE J. Sel. Top. Quantum Electron. **5**, 808 (1999).